Capillary stretching of fibers

C. Duprat[1] and S. Protiere[2,3]

[1] *Laboratoire d'Hydrodynamique (LadHyX), Ecole Polytechnique - F-91128 Palaiseau Cedex, France*
[2] *CNRS, UMR 7190, Institut Jean Le Rond d'Alembert - F-75005, Paris, France*
[3] *Sorbonne Universites, UPMC Univ Paris 06, UMR 7190, Institut Jean Le Rond d'Alembert*
F-75005, Paris, France

Abstract – We study the interaction of a finite volume of liquid with two parallel thin flexible fibers. A tension along the fibers is imposed and may be varied. We report two morphologies, *i.e.* two types of wet adhesion: a weak capillary adhesion, where a liquid drop bridges the fibers, and a strong elastocapillary adhesion where the liquid is spread between two collapsed fibers. We show that geometry, capillarity and stretching are the key parameters at play. We describe the collapse and detachment of the fibers as a function of two nondimensional parameters, arising from the geometry of the system and a balance between capillary and stretching energies. In addition, we show that the morphology, thus the capillary adhesion, can be controlled by changing the tension within the fibers.

At small scales, surface tension produces large adhesion forces. A classical example of such capillary adhesion is the adhesion of two wet spheres. When the spheres are elastic, their deformation increases the contact area and thus the adhesion force [1]. Another example of capillary adhesion enhanced by elasticity consists in a drop bridging the gap between two soft substrates. In that case, surface tension deforms the substrates, reducing the height gap, which leads to an increase in Laplace pressure, thus a magnified adhesion [2]. These elastic deformations mediated by surface tension fall into a category of problems called *elastocapillarity* [3]. Capillary forces cause elastic deformations that occur through bending and/or stretching. For example capillary-bending coupling is responsible for the wrapping of a thin sheet around a drop [4] or the aggregation of wet fibers [5–7]. On the other hand, it is a capillary-stretching balance that controls the wrinkles appearing when a drop is deposited on a thin floating sheet or when a sheet is deposited on a drop [8–10]. Mastrangelo and Hsu have considered both bending and stretching to describe the surface-tension–mediated collapse of doubly clamped beams in the context of MEMS [11–13]. However, the elastocapillary adhesion of thin elongated objects in situations where stretching dominates has been overlooked despite its relevance in the wetting of fibrous media.

As a prototype to study such stretching-capillary systems, we consider the simple case of clamped thin elongated fibers (radius r, length L, such that $\beta = r/L \ll 1$) separated by a distance $2d$ and wetted by a liquid as shown in fig. 1(a). When the fibers are rigid, the shape of the liquid between them is solely governed by a minimization of surface energy with a single control parameter d/r; below a critical distance d_m/r, the liquid spontaneously spreads into a long column [14,15]. In the general case of deformable fibers (of Young's modulus E), there is also an elastic energy cost. The elastic energy consists in a combination of bending $\mathcal{E}_b \approx EId^2/L^3$, where $I = \pi r^4/4$ is the second moment of area, and stretching $\mathcal{E}_s \approx Td^2/L$, where $T = E\epsilon\pi r^2$ is the tension force due to a pre-strain ϵ within the fibers. This pre-strain is much greater than the typical deformation $(d/L)^2$, thus the tension remains constant when the fibers are deformed. In our system of large aspect ratio fibers, most of the energetic cost comes from stretching and bending can be neglected $(\mathcal{E}_s/\mathcal{E}_b = 4\epsilon(L/r)^2 \gg 1)$.

The setup is sketched in fig. 1(a). We mold elastomeric fibers (polyvinylsiloxane, Zhermack Elite Double) of various Young's moduli E, lengths L and radii r. A system consisting of four micro-controlled platforms enables to adjust the strain ϵ within the fibers and the inter-fiber
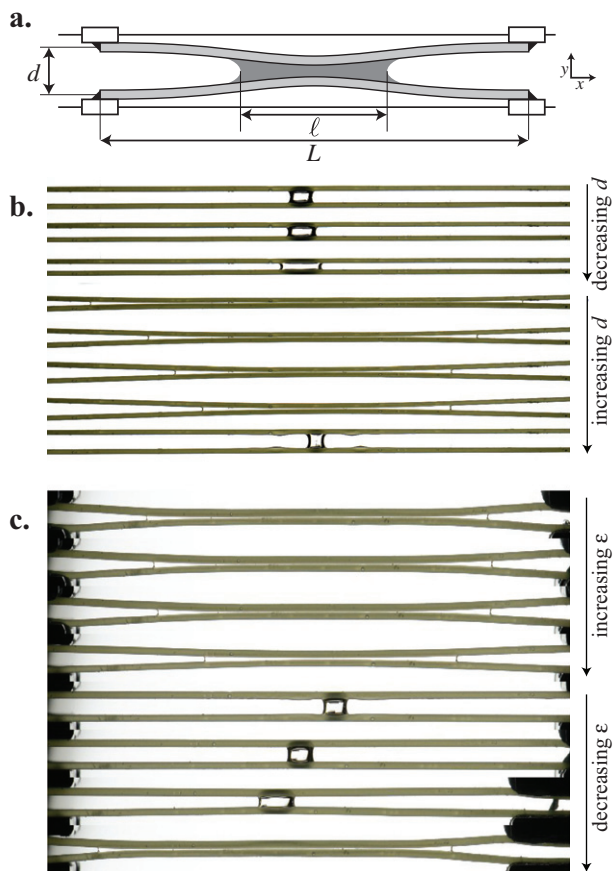
Fig. 1: (Colour on-line) (a) Schematic of the setup. (b) Evolution of a drop on two parallel flexible fibers ($r = 0.2\,\text{mm}$) as the distance between the fibers is varied and (c) as the tension of both fibers is varied. PVS fibers of radius $r = 0.3\,\text{mm}$, $L = 5\,\text{cm}$, $E = 0.9\,\text{MPa}$, drop volume $V = 3\,\mu\text{L}$.

distance $2d$. Each fiber is attached at its ends on two independent platforms to control the strain along the x-axis. Both fibers are then mounted individually on another platform to adjust the inter-fiber distance incrementally along the y-axis. The fibers are kept parallel and at the same height. A drop of mineral oil (surface tension $\gamma = 30\,\text{mN/m}$, contact angle $\theta_{eq} = 5°$) of volume V is placed between the fibers. We know that on rigid fibers, the critical spreading distance d_m/r is independent of the volume provided that $V/r^3 < 700$ [14]. In our experiments, we thus keep the volume constant and $V = 3\,\mu\text{L}$, *i.e.* $V/r^3 < 400$.

A first set of experiments consists in varying the distance d while keeping L and ϵ constant (fig. 1(b)). As the distance d decreases, the length of the drop slightly increases. At a critical inter-fiber distance, the fibers are pulled together and undergo a strong deformation resulting in a rapid spreading of the liquid. In the center, the fibers are straight and almost in contact over a distance approximatively corresponding to the wetted length. The deformation is concentrated in the region between the clamped edges and the menisci. We call this rapid change of shape a "zipping" transition. By increasing d

incrementally, we pull the fibers apart along the y-axis (fig. 1(b)). The straight portion of the fibers decreases. At a critical distance, the fibers "unzip".

A second set of experiments consists in keeping the inter-fiber distance constant and pulling the fibers along the x-axis, thus varying both L and ϵ (fig. 1(c)). Zipping and unzipping transitions are obtained by controlling the tension applied to the fibers: when the tension is decreased, the drop spreads and zips the fibers, while when the tension is increased, the fibers separate.

For both types of experiments we measure the wetted length ℓ, *i.e.* an estimate of the extent of the deformation, as d or ϵ is varied. For two typical experiments we report its evolution in fig. 2(a). All lengths are made nondimensional with r. The data indeed show that the liquid adopts either the shape of a short drop ($\ell/r \sim 20$) or of a long zipped column ($\ell/r \sim 150$). Both curves display the same reversible hysteretic behavior: a sudden collapse of the fibers at a minimum value of d/r or ϵ and a rapid detachment at a maximum value of the parameters. Below the minimal value i) the fibers are always zipped, above the maximal value ii) only drops prevail and thus for intermediate values iii) both states coexist. Two different actions, stretching the fibers axially or pulling them apart transversally, lead to analogous results.

The liquid/fibers interaction depends on all the physical parameters of the system: L, d, r, E, ϵ and γ. In order to construct a phase diagram, we fix the fiber length. This allows us to identify two dimensionless parameters, a geometric parameter d/r and a capillary-stretching number $\mathcal{N}_{cs} = E\epsilon r/\gamma$. This parameter is reminiscent of the characteristic dimensionless number Eh/γ found for stretched plates of thickness h [16,17]; in our case the typical length is the fiber radius r and the Young modulus is replaced by an effective modulus $E\epsilon$ that does not only depend on the material properties but can also be tuned by adjusting the tension. The resulting phase diagram is shown in fig. 2(b). Five regions emerge.

The region where only drops exist is labeled D. For large values of d/r (hatched region N) the fibers are too far apart for any capillary bridge to bind them. For small values of d/r the fibers are always zipped (region Z_1). We find an intermediate region where the drop and the zipped fibers configurations are possible. This coexistence region, labeled DZ, increases rapidly with decreasing tension. Finally, for small values of $\mathcal{N}_{cs}$ a second zipped-fibers region, labeled Z_2, appears for large values of d/r, above the limit of capillary-bridge breakup.

In the region Z_2, the fibers can sustain large deformations, *i.e.* a large inter-fiber distance d is required to pull them apart (fig. 2(c)). After unzipping, no capillary bridge remains; the reversibility is lost. In this case the hysteretic cycle is broken (fig. 2(d)): the region is only accessible through the DZ region while in a zipped state. The fiber flexibility extends capillary adhesion to inter-fiber distances impossible to reach with rigid fibers.
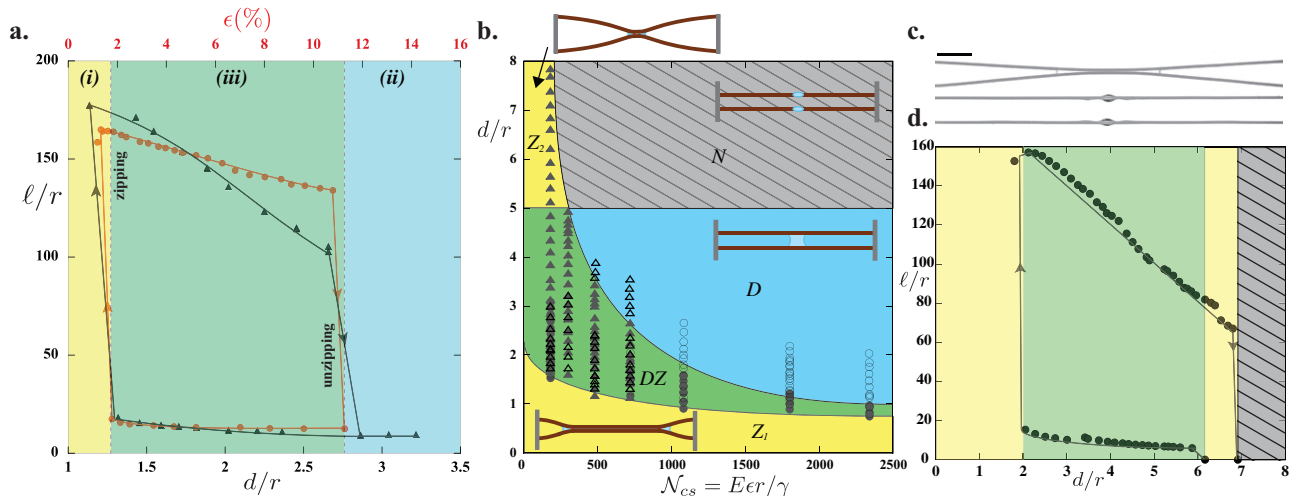
Fig. 2: (Colour on-line) (a) Evolution of the length of a drop ℓ/r when the inter-fiber distance d/r (▲) or the tension ϵ (●) is varied. The arrows indicate the direction of the hysteretic loop and the dashed lines are guides for the eyes. PVS fibers of radius $r = 0.2$ mm, $L = 5$ cm, $E = 0.9$ MPa, drop volume $V = 3\,\mu$L. (b) Morphology diagram in the parameter space $(d/r,\ E\epsilon r/\gamma)$: drops (open symbols) or columns (filled symbols) for $r = 0.2$ and 0.3 mm, $L = 5$ cm, $E = 0.5$ and 0.9 MPa. There are five regions: columns only (Z_1 and Z_2), drops only (D), coexistence of states (DZ) and no liquid bridge (grey hatched region). (c) Liquid morphology in the Z_2 region as d/r increases ($E\epsilon r/\gamma = 172.5$, $d/r > 6$). Scale bar: 5 mm. (d) Evolution of the wetted length ℓ/r as a function of the distance d/r for $E\epsilon r/\gamma = 172.5$ ($r = 0.2$ mm, $E = 0.9$ MPa, $\epsilon = 2.5\%$ and $L = 5$ cm).

Finally, experiments show that all boundaries are independent of the drop volume, except for the boundary of the N region, which is given by $d \approx 0.9V^{1/3}$ since in this case the drop is nearly spherical.

We can thus distinguish two types of adhesion: a weak capillary adhesion (*i.e.* drops D) and a strong elastocapillary adhesion (*i.e.* zipped columns Z). We first focus on the unzipping of the fibers, *i.e.* the upper boundary of the elastocapillary adhesion region DZ and Z_2 ($DZ \to D$ and $Z_2 \to N$). We use a simplified model to describe the zipped fibers (inset of fig. 3): the deformation of the fibers is confined to the dry region of length L_{cs} while the wet portion is considered undeformed. In this flat region the fibers are coalesced and the liquid exerts a capillary force $F_\gamma \sim \gamma\ell$. The total energy reads

$$\mathcal{E}_{total} = \mathcal{E}_e + \mathcal{E}_\gamma \sim E\epsilon\pi r^2 \frac{d^2}{L_{cs}} - \gamma r(L - 2L_{cs}). \quad (1)$$

The equilibrium configuration is given by a minimization of the total energy ($d\mathcal{E}_{total}/dL_{cs} = 0$), which yields for the dry length

$$L_{cs} \sim d\sqrt{\mathcal{N}_{cs}}. \quad (2)$$

As observed experimentally, this relation demonstrates that L_{cs} increases linearly with the inter-fiber distance and with the increasing tension (fig. 2(a) and (d)). We consider that detachment occurs when L_{cs} reaches $L/2$. This condition can be written as

$$\frac{d}{L} \sim \frac{1}{\sqrt{\mathcal{N}_{cs}}}. \quad (3)$$

$\mathcal{N}_{cs}$ represents the intrinsic material properties (size r, effective elasticity $E\epsilon$, surface tension γ); it quantifies the
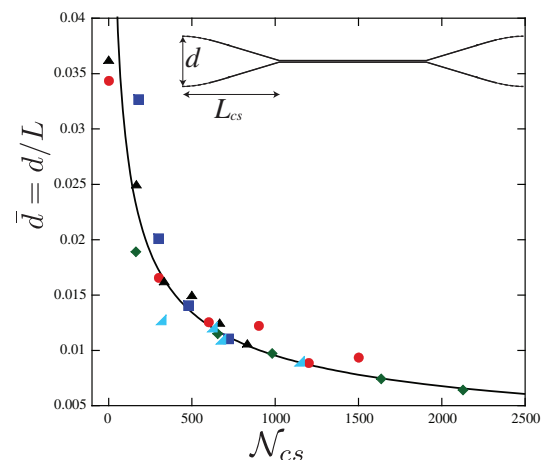

Fig. 3: (Colour on-line) Detachment of the column, for $L = 4$ cm, $r = 0.2$ mm, $E = 0.4$ MPa (▲) and $E = 0.9$ MPa (●); $E = 0.9$ MPa, $L = 5$ cm, $r = 0.2$ mm (■) and $r = 0.3$ mm (◆); obtained by changing the distance d and by varying the tension).

amount of deformation that can be sustained by capillary forces. The aspect ratio d/L corresponds to the imposed geometry, thus describes the deformation. We perform experiments either by separating the fibers along the y-axis or by pulling on the fibers along the x-axis, for several fiber moduli E, lengths L and radii r, thus varying both $\mathcal{N}_{cs}$ and $\bar{d} = d/L$. The points of detachment are reported in fig. 3. The data collapse onto a single curve given by eq. (3) with a prefactor 0.3. This constant prefactor confirms that detachment occurs when L_{cs} is equal to a fixed fraction of L. However this fraction (0.3) is slightly smaller

than 1/2 probably due to a dynamical process (see supplementary material `movie1_unzippingV2.mov`[1]). Below the curve, the capillary forces are sufficient to keep the fibers together attached at their center. At large $\mathcal{N}_{cs}$, capillary forces are weak and fibers are rigid-like, so that only small deformations can be sustained. At large aspect ratios $\bar{d}$, strong capillary forces (or highly flexible fibers) are necessary to keep the fibers attached.

We now study the zipping transition, *i.e.* the boundary of the Z_1 region in fig. 2(b). This boundary corresponds to $d/r \simeq d_m/r = \sqrt{2}$ and is only slightly dependent on $\mathcal{N}_{cs}$. This transition is due to the spreading of the drop into a column at a critical d/r as in the rigid case [14]. However, in this case, the flexibility induces the collapse of the fibers resulting in the zipped state. To understand this zipping, we look at the dynamics presented in fig. 4(a). Experimentally, we vary either d or $\mathcal{N}_{cs}$ incrementally until we reach the boundary Z_1. At $t = 0$, d or $\mathcal{N}_{cs}$ is now fixed and we record the spontaneous dynamics of the drop (see supplementary material `movie2_zippingV2.mov`[2]). The drop starts to spread slowly while the distance between the fibers at the center d_0 remains nearly constant. A sudden collapse of the fibers occurs and the liquid spontaneously spreads in less than 10 s. Finally, the liquid continues spreading until the equilibrium shape is reached. We can distinguish two time scales: a slow capillary spreading and a rapid elastic collapse. We note that at high $\mathcal{N}_{cs}$, *i.e.* for rigid-like fibers, the drop first spreads into a column while the fibers remain unzipped; the zipping transition is then similar, with a slow spreading of the column followed by a rapid elastic collapse. The zipping process is a dynamical one. Capillarity causes spreading of the liquid. During this spreading, the capillary forces $\sim \gamma\ell$ increase with the liquid length and the distance d_0 decreases. We determine the onset of collapse by taking the inflection point of the curve $\ell(t)$ (fig. 4(a)). At this critical zipping time, we measure the wetted length $\ell = \ell_{zip}$ and the interfiber distance at the center $d_0 = d_z$. For a given radius d_z is approximatively constant and given by $d_z/r \approx 0.6$. Looking at the shape of the column cross-section as described by Princen [14,15] (fig. 4(b)), we notice that there is a transition between a concave ($R > 0$) and convex ($R < 0$) interface and a variation in the position of the contact line (from $\alpha > \pi/2$ to $\alpha < \pi/2$) at $d_0/r = 0.57$. This shape transition is the onset of the rapid spreading of the liquid, thus the fast collapse of the fibers.

The zipping therefore occurs when the force applied by the liquid is large enough to bring the fibers together at a distance $d_z/r \approx 0.6$. Assuming the capillary force is equivalent to a point force applied at the center of the fibers with a magnitude $\gamma\ell$, a force balance on the fiber gives

$$2T\sin\phi = \gamma\ell, \tag{4}$$

[1]Movie presenting the dynamics of two PVS fibers ($E = 0.9$ MPa) unzipping, $r = 0.2$ mm, $\epsilon \approx 0.1\%$ and $d/r = 30$.
[2]Movie presenting the dynamics of two PVS fibers ($E = 0.9$ MPa) zipping, $r = 0.2$ mm, $\epsilon \approx 0.1\%$ and $d/r = 11$.
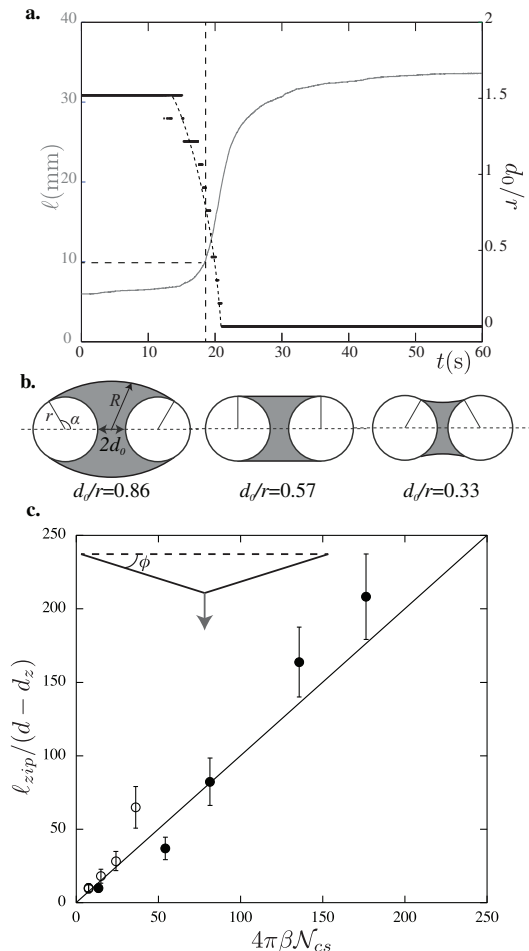

Fig. 4: (a) Evolution of the liquid length $\ell(t)$ and the inter-fiber distance at the center $d_0(t)$ at the zipping transition; $L = 5$ cm, $r = 0.3$ mm, $\epsilon = 8\%$, $E = 0.9$ MPa. (b) Theoretical shape of the cross-section of the column for $d_0/r = 0.86$ ($\alpha = 2\pi/3$, $R/r = 4.7$), $d_0/r = \pi/2 - 1 \simeq 0.57$ ($\alpha = \pi/2$, $R/r = \infty$), and $d_0/r = 0.33$ ($\alpha = \pi/3$, $R/r = -1.7$). (c) Zipping transition (open symbols: $r = 0.2$ mm, filled symbols: $r = 0.3$ mm).

where $T = T_0 = E\epsilon\pi r^2$ is the tension within the fiber and ϕ is the angle of deformation (sketch in fig. 4(c)). At zipping, $\phi \approx 2(d - d_z)/L$, $\ell = \ell_{zip}$ and we find

$$\frac{\ell_{zip}}{d - d_z} = 4\pi\beta\mathcal{N}_{cs}. \tag{5}$$

We measure ℓ_{zip} for several fiber radii, lengths, various strains, and by decreasing d/r (fig. 1(b)) or decreasing the tension T (fig. 1(c)). We plot $\ell_{zip}/(d - d_z)$ as a function of $4\pi\beta\mathcal{N}_{cs}$. The data collapse on a line of slope 1, in good agreement with (5).

Like the unzipping transition, the dynamic zipping process is rationalized with a combination of geometry (ℓ/d) and material properties ($\mathcal{N}_{cs}$).

To summarize, the interaction of a liquid with thin flexible fibers leads to a strong elastocapillary adhesion. Geometry, capillarity and stretching are the key parameters at play via the aspect ratio d/L (or d/ℓ) and

the capillary-stretching number $\mathcal{N}_{cs} = E\epsilon r/\gamma$. Collapse or detachment can thus be controlled by varying the effective modulus $E\epsilon$ which is possible by applying an external strain. This external action may then promote adhesion or limit failure, and could be extended to tune drying rate [18] and to optimize liquid capture on fiber arrays. Moreover, this experiment corresponds to a realistic model system for constrained fibers as found in woven or entangled fibrous media and could give new insights on the wetting and shrinking of complex filters, membranes and textiles [19].

$$* * *$$

REFERENCES

[1] Butt H.-J., Barnes W. J. P., del Campo A., Kappl M. and Schönfeld F., *Soft Matter*, **6** (2010) 5930.

[2] Wexler J. S., Heard T. M. and Stone H. A., *Phys. Rev. Lett.*, **112** (2014) 066102.

[3] Roman B. and Bico J., *J. Phys.: Condens. Matter*, **22** (2010) 493101.

[4] Py C., Reverdy P., Doppler L., Bico J., Roman B. and Baroud C., *Phys. Rev. Lett.*, **98** (2007) 2.

[5] Py C., Bastien R., Bico J., Roman B. and Boudaoud A., *EPL*, **77** (2007) 44005.

[6] Pokroy B., Kang S. H., Mahadevan L. and Aizenberg J., *Science*, **323** (2009) 237.

[7] Duprat C., Protière S., Beebe A. Y. and Stone H. A., *Nature*, **482** (2012) 510.

[8] Huang J., Juszkiewicz M., de Jeu W. H., Cerda E., Emrick T., Menon N. and Russell T. P., *Science*, **317** (2007) 650.

[9] Vella D., Adda-Bedia M. and Cerda E., *Soft Matter*, **6** (2010) 5778.

[10] King H., Schroll R. D., Davidovitch B. and Menon N., *Proc. Natl. Acad. Sci. U.S.A.*, **109** (2012) 9716.

[11] Mastrangelo C. H. and Hsu C. H., *J. Microelectromech. Syst.*, **2** (1993) 33.

[12] Mastrangelo C. H. and Hsu C. H., *J. Microelectromech. Syst.*, **2** (1993) 44.

[13] Mastrangelo C., *Tribol. Lett.*, **3** (1997) 223.

[14] Protiere S., Duprat C. and Stone H. A., *Soft Matter*, **9** (2013) 271.

[15] Princen H., *J. Colloid Interface Sci.*, **34** (1970) 171.

[16] Chopin J., Vella D. and Boudaoud A., *Proc. R. Soc. A: Math., Phys. Eng. Sci.*, **464** (2008) 2887.

[17] Hure J., Roman B. and Bico J., *Phys. Rev. Lett.*, **106** (2011) 174301.

[18] Duprat C., Bick A. D., Warren P. B. and Stone H. A., *Langmuir*, **29** (2013) 7857.

[19] Kamo J., Hiram T. and Kamada K., *J. Membr. Sci.*, **70** (1992) 217.